Dynamic Skyrmion-Mediated Switching of Perpendicular MTJs: Feasibility Analysis of Scaling to 20 nm with Thermal Noise

Md Mahadi Rajib, Walid Al Misba, Dhritiman Bhattacharya, Student Member, IEEE, Felipe Garcia-Sanchez, Member, IEEE and Jayasimha Atulasimha, Senior Member, IEEE.

Abstract—One method of creating and annihilating skyrmions in confined geometries is to use Voltage-Controlled Magnetic Anisotropy (VCMA) [1, 2, 3]. Previous study shows that robust voltage controlled ferromagnetic reversal from "up" to "down" state in the soft layer of a perpendicular Magnetic Tunnel Junction (p-MTJ) can be achieved by creating and subsequently annihilating an intermediate skyrmion state [4] in the presence of room temperature thermal noise and anisotropy variation across grains [4]. However, when scaling to 20 nm, thermal noise can annihilate the skyrmions, for example, by randomly moving the core towards the boundary of the nanostructure. In this work, we study three p-MTJs of different dimensions, specifically lateral dimensions of 100nm, 50nm and 20 nm and investigate the change in switching behavior as the dimension is decreased. Particularly, we show that while skyrmion mediated switching of ferromagnets in the presence of thermal perturbation is feasible down to lateral dimensions ~20nm, the large values of VCMA and DMI needed at ~20nm lateral dimensions have only been theoretically predicted and are yet to be experimentally demonstrated to date.

Index Terms—Nanomagnetic devices, VCMA, Skyrmion-mediated switching, MRAM, Energy efficient, non-volatile memory.

I. INTRODUCTION

Typically, nanomagnetic memory elements are based on perpendicular Magnetic Tunnel Junctions (p-MTJ) as shown in Fig. 1 (a). The magnetoresistance of an MTJ can be changed by switching the magnetization direction of the free layer between two stable orientations (i.e. writing a memory bit), which in turn allows reading out of the memory bit [5-8].

Various current induced [9-13] and electric fieldcontrolled [14-22] mechanisms can be used for switching the free layer of an MTJ. Spin transfer torque (STT) [9, 10], one of the most commonly employed current controlled switching strategies, causes a large energy dissipation (~100fJ/bit). For comparison, energy dissipated in CMOS devices is approximately 100 aJ/bit [23], which is nearly three orders of magnitude lesser than energy dissipated in STT based switching. On the other hand, electric fieldinduced magnetization reversal is highly energy efficient. In particular, Voltage Controlled Magnetic Anisotropy (VCMA) based switching dissipates only ~1fJ/bit [18, 24]. In this method, a voltage pulse alters the perpendicular magnetic anisotropy originating at the interface of ferromagnet/oxide [25]. Utilizing an appropriate combination of in-plane bias magnetic voltage pulse duration, complete and ferromagnetic reversal can be achieved [15]. However, VCMA induced switching is precessional in nature and highly susceptible to disorders in the presence of room-temperature thermal noise [4].

Recently, the possibility of VCMA induced magnetization reversal between two ferromagnetic states without any external bias magnetic field has been reported [4]. This is achieved by applying a voltage pulse that reduces PMA. Thus, starting from one of the ferromagnetic states (up/down), an intermediate skyrmion can be created. The voltage pulse is withdrawn coincidentally with the inbreathing motion of the skyrmion. Due to this, when the initial PMA value is restored, the intermediate skyrmion annihilates to the other [4] ferromagnetic state (down/up). The switching mechanism is shown in Fig. 1(b). Skyrmions are usually controlled by electrical current in racetrack devices which was proven to be

Submitted on March xx, 2020. M. M. R., D.B. and J.A. are supported by NSF SHF Small Grant #1909030.

M. M. Rajib, W. Misba and D. Bhattacharya are with the Department of Mechanical and Nuclear Engineering, Virginia Commonwealth University, Richmond, VA 23284 USA (e-mail: rajibmm@mymail.vcu.edu, misbawa@mymail.vcu.edu and bhattacharyad@vcu.edu).

F. Garcia-Sanchez is affiliated with Departamento de Física Aplicada, University of Salamanca, Pza de la Merced s/n, 37008 Salamanca, Spain (f.garcia@inrim.it)

J. Atulasimha is with the Department of Mechanical and Nuclear Engineering and the Department of Electrical and Computer Engineering, Virginia Commonwealth University, Richmond, VA23284 USA (e-mail: jatulasimha@vcu.edu)

advantageous due to its potential in overcoming edge roughness related pinning occurring in Domain Wall (DW) based racetrack devices [26-28]. However, the skyrmion-mediated switching strategy explored in this paper uses a confined geometry and thus has potential for higher density memory cells compatible with crossbar architecture. This mechanism has been shown to be robust to thermal noise, disorder and perturbative spin currents for a nanomagnet of lateral dimension 100nm. However, to be competitive with the current miniaturization trend in Spin Transfer Torque Random Access Memory (STTRAM), further downscaling is required. In this work, we theoretically investigate the feasibility of downscaling the skyrmion mediated switching scheme by studying three MTJs of different sizes, 100nm, 50 nm and 20 nm respectively. We observe that with the reduction in lateral dimension with concomitant scaling of the thickness, high perpendicular magnetic anisotropy, high DMI and a larger VCMA coefficient are required for successful operation of the device. The breathing frequency of skyrmions in the downscaled nanomagnets is high leading to switching frequency ~1 GHz, ~10 GHz, ~100 GHz for 100 nm, 50 nm and 20 nm respectively. Thus, as one scales to lateral dimension less than 50 nm, there is likely to be a very narrow range of pulse width where the switching is robust in the presence of thermal noise. Additionally, material parameters required along with their feasibility, switching error, etc., are studied in this paper. Section II of this paper discusses the method followed for numerical simulations in this study. Section III describes the findings from this study and Section IV makes concluding remarks based on the numerical simulations on potential scaling in skyrmion mediated switching of p-MTJs.

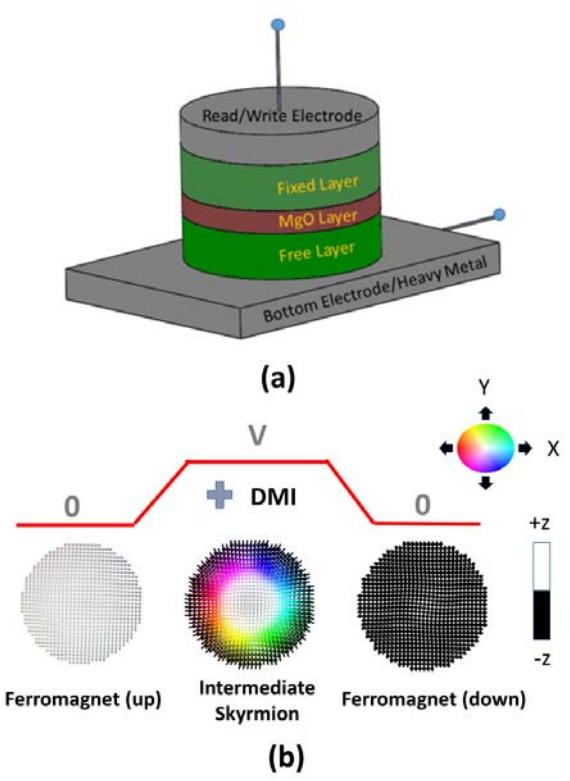


Fig. 1: (a) Schematic of a Magnetic Tunnel Junction and (b) Energy barrier separates the two non-volatile perpendicular stable states (ferromagnetic up and down states) at equilibrium (V=0). In the presence of DMI in the free layer, reducing PMA with the VCMA effect on application of a voltage (V) creates a skyrmion. By withdrawing the voltage coincidentally with the in breathing of skyrmion, reversal of ferromagnetic state is achieved. Corresponding states (ferromagnetic up, down and skyrmion) are shown below the voltage pulse.

II. METHOD

We simulate the magnetization dynamics of the free layer of the MTJs, which were discretized into 64×64×1, 32×32×1 and 16×16×1 cells for 100nm, 50nm and 20nm MTJs respectively to keep the lateral (in-plane) discretization similar to the extent possible. The magnetization dynamics is simulated by solving the Landau-Lifshitz-Gilbert (LLG) equation via the micromagnetic simulation software Mumax3 [29]:

$$\frac{\partial \vec{m}}{\delta t} = \left(\frac{-\gamma}{1 + \alpha^2}\right) \left[\vec{m} \times \vec{B}_{eff} + \alpha \left\{ \vec{m} \times \left(\vec{m} \times \vec{B}_{eff} \right) \right\} \right]$$
 (1)

In eqn (1), γ is the gyromagnetic ratio (rad/Ts), α is the Gilbert damping coefficient. \vec{m} is the normalized magnetization vector, found by normalizing the magnetization vector (\vec{M}) with respect to saturation magnetization (M_s) and \vec{B}_{eff} is the effective magnetic field with the following components [29]:

$$\vec{B}_{eff} = \vec{B}_{demag} + \vec{B}_{exchange} + \vec{B}_{dm} + \vec{B}_{anis} + \vec{B}_{thermal} \tag{2}$$

 \vec{B}_{demag} is the effective field due to demagnetization energy, $\vec{B}_{exchange}$ is the effective field due to the Heisenberg exchange interaction and \vec{B}_{dm} is the effective field due to Dzyaloshinskii-Moriya interaction.

The effective field due to the perpendicular anisotropy, \vec{B}_{anis} is given by the following equation:

$$\vec{B}_{anis} = \frac{2K_{u1}}{M_s} (\vec{u}.\vec{m})\vec{u} + \frac{4K_{u2}}{M_s} (\vec{u}.\vec{m})^3 \vec{u}$$
 (3)

 K_{u1} and K_{u2} are the first and second order uniaxial anisotropy constants and \vec{u} a unit vector in the anisotropy direction. VCMA induced PMA modulation is employed by modulating K_{u1} while keeping $K_{u2} = 0$.

Thermal field contribution to the effective field is calculated by:

$$\vec{B}_{thermal} = \vec{\eta}(step) \sqrt{\frac{2\alpha k_B T}{M_s \gamma \Delta V \Delta t}}$$
(4)

 k_B the Boltzman constant, T the temperature, ΔV the cell volume, Δt is time step which is considered to be 10fs for all of our simulation cases (reason explained in the appendix) and $\vec{\eta}(step)$ a random vector from a standard normal distribution whose value is changed after every time step.

III. RESULTS AND DISCUSSION

Our proposed structure is presented in Fig. 1(a). The free layers were chosen to be nanodisks of diameter 100 nm, 50 nm and 20 nm. The thickness to diameter ratio (the aspect ratio) was set to 0.012 for 100nm and 50nm MTJs in order to maintain constant demagnetization factor. However, 0.6 nm thickness was kept unchanged for scaling from diameter of 50 nm to 20 nm instead of reducing it to 0.24 nm as such a low thickness would make the device impractical. We considered exchange stiffness A=25 pJ/m, saturation magnetization M_s=1.3×10⁶ A/m, Gilbert damping coefficient α=0.01. For successful realization of our switching mechanism, we require an initial ferromagnetic state. Next, when the PMA is reduced (voltage applied), we need to form an intermediate skyrmion state to provide a robust pathway for magnetization reversal to the opposite ferromagnetic state when the PMA is restored (voltage withdrawn). We varied the perpendicular anisotropy (K_{ul}) and the DMI parameter (D) to fulfill these requirements. The

rationale behind choosing different anisotropy and DMI values is discussed below.

Firstly, to form the intermediate skyrmion state, we need a sizeable DMI. Moreover, reduction of lateral dimension requires higher DMI to form an intermediate skyrmion state. However, to maintain an initial ferromagnetic state, the DMI value must be less than the critical value ($D_{crit} = \frac{4}{\pi} \sqrt{AK_{EFF}}$, where $K_{EFF} = K_{ul} - \frac{1}{2} \mu_0 M_s^2$) at the corresponding initial PMA value. Here, K_{EFF} is the effective perpendicular anisotropy and the D_{crit} (critical DMI) value signifies a threshold beyond which a metastable skyrmion can be formed in the system

Energy barrier between two ferromagnetic states reduces due to the presence of DMI [30]. To incorporate this reduction, we have estimated the energy barrier with K_{eff} from the phenomenological equation $K_{eff} = (K_{u1} - \frac{1}{2} \, \mu_0 M_s^2 - \frac{D^2 \pi^2}{16A})$. The perpendicular anisotropy is determined from the thermal stability factor $K_{eff}V/k_BT$, which was considered to be appropriately around 50 for all three MTJs. Therefore, with reduction of lateral dimension, required DMI increases and consequently the uniaxial anisotropy K_{u1} needs to be increased to ensure thermal stability with an energy barrier of $\sim 50 \, k_BT$.

With the reduced thickness of 0.6 nm in cases of 50nm and 20 nm along with high PMA, pinning effect can be present [31]. However, we do not consider the pinning effect as this is a feasibility study and including the effect of defects is beyond the scope of this paper. Moreover, stray field from the fixed layer of the MTJ can assist in skyrmion formation [32, 33]. Nevertheless, a small field in either the perpendicular or any of the in-plane directions does not significantly affect the switching dynamics [4]. Therefore, we did not include stray field in our simulations.

The parameters are listed in Table I (A=25 pJ/m, M_s =1.3×10⁶ A/m, α =0.01 for all cases):

TABLE I

MTJs	K_i $(\mu J/m^2)$	Energy barrier (k _B T)	D_{crit} (mJ/m^2)	$D \over (mJ/m^2)$
100nm	1332	45.55	1.42	1.2
50nm	1044	51.32	5.25	4.5
20nm	3798	50.09	14.61	13.0

We note that the feasibility of the material parameters such as PMA (K_i) and DMI coefficient (D) in Table I

(and also the VCMA coefficients mentioned on Table II later) are discussed in the conclusion section.

A. Non-thermal

First, we study the behavior of the nanomagnets by reducing PMA through VCMA without any thermal perturbation. At reduced PMA, the competing PMA, DMI and demagnetization forms a skyrmion. Once the skyrmion is formed, it starts to oscillate between two stable states: skyrmionic state and quasi-ferromagnetic state. The oscillation is observed in the form of topological charge evolution with time (Fig. 2) where the crests indicate a skyrmionic state and troughs indicate a quasi-ferromagnetic state. With the reduction of lateral dimension, the DMI required to form an intermediate skyrmion state increases. Thus, it forces the magnetization to oscillate at a higher frequency. This reduces the pulse width and the rise time of the voltage pulse applied that can produce favorable switching in the smaller nanomagnets. VCMA coefficients, fall and rise time, total change in PMA, oscillation frequency and pulse-width range are listed in Table II considering application of voltage pulse (ΔV) of 2.0 V across 1 nm thick MgO layer for all three MTJs.

TABLE II (Columns 2-4 are parameters chosen and column 5, 6 are inferred from simulations)

MTJs	VCMA	Fall/	ΔK_i	Pulse-	Osc.
	Coeff.	rise	$(\mu J/m^2)$	width	Freq.
	(fJ/Vm)	time		range	(GHz)
	,	(ps)		(ps)	(-)
		(1-)		(F ~)	
100nm	102	100	204	500-900	~1
50nm	252	1	504	22-102	~8
20nm	1569	0.5	3138	4-13	~60

By withdrawing the voltage pulse and restoring the PMA to the initial values at each peak point, switching is observed. When PMA is restored, the intermediate skyrmions are collapsed and go to either the opposite ferromagnetic state or back to the initial ferromagnetic state due to the minimization of curvature energy ($\sigma = 4\sqrt{AK_{EFF}} - \pi D$) of the 360° domain wall of the skyrmion's spin spiral [34]. In addition to this, we exploit in breathing dynamics to ensure the resulting ferromagnetic state is opposite the initial state resulting in the skyrmion mediated reversal. Fig. 2 shows that the nanomagnets switch for the first 5, 5 and 7 cycles respectively for 100 nm, 50 nm and 20

nm lateral dimension (diameter) nanomagnets. Beyond these cycles (for respective nanomagnet sizes), the topological number falls below the critical value and therefore an intermediate skyrmion state is not available for successful switching. The "switch" and "no switch" regions along with the comparison of topological evolution for three nanomagnets are shown in Fig. 2. By the "switch" region we mean that when the voltage pulse is withdrawn (PMA restored) roughly at the maxima of the topological charge in Fig. 2, the magnetization of the nanomagnet relaxes to a ferromagnetic state that is opposite (reversed) from the original state. In other words, the switching or reversal is successful. In the "no switch" region, even if the voltage pulse is withdrawn (PMA restored) roughly at the maxima of topological charge the magnetization relaxes to the original ferromagnetic state and thus does not switch successfully.

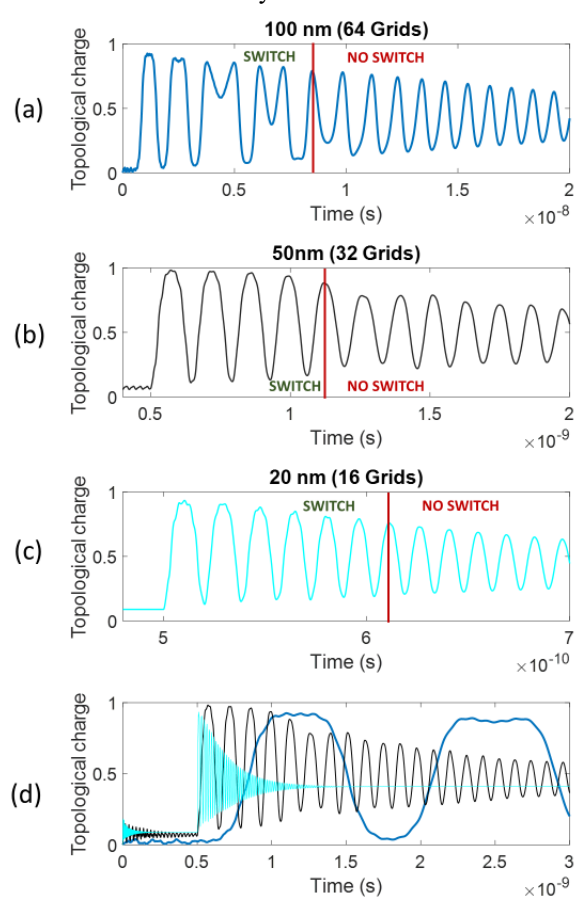


Fig. 2: "Switch" and "no switch" region without thermal perturbation for (a) 100nm (b) 50 nm (c) 20 nm and (d) Comparison of topological evolution of three nanomagnets using same time scale for the nanomagnets of three different sizes.

B. Thermal

In the presence of room temperature thermal noise, the first breathing period of skyrmion is ideal for the switching to minimize the possibility of intermediate skyrmion annihilation due to thermal noise. The switching percentage for 100 nm nanomagnet with pulse width range of 400-700 ps is studied and shows thermally robust switching in the 450-650 ps range (Fig. 3a). For 50 nm, thermally robust switching is observed for the pulse width range of 32-42 ps by studying the switching percentage in the pulse width range of 22-102 ps (Fig. 3b). For 20 nm, switching percentage is studied for pulse width range of 4-13 ps. Within this range, 99% switching is observed in the pulse width range of 6-7ps (Fig. 3c).

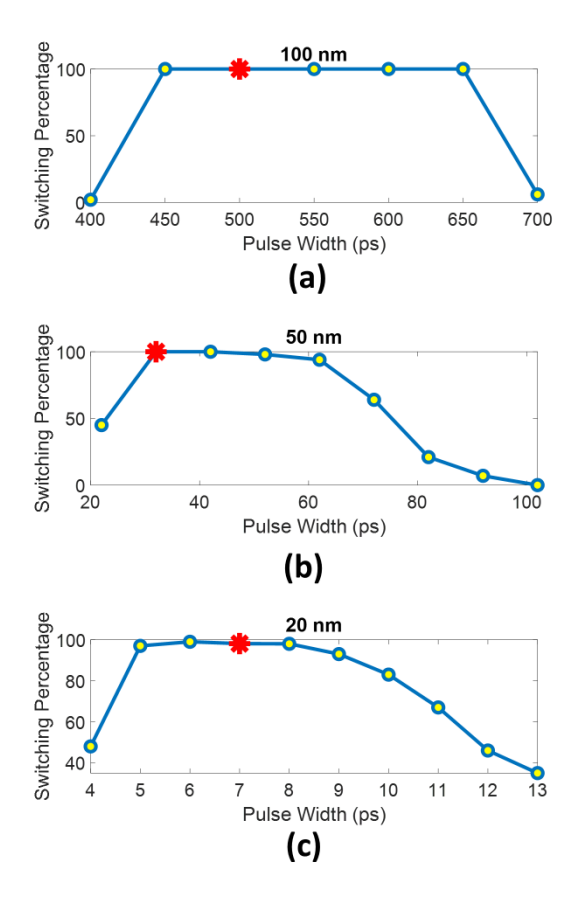


Fig. 3: Switching probability vs. pulse width of (a) 100nm (b) 50nm and (c) 20 nm nanomagnets. [For studying the switching percentage for different pulse widths, the simulations were run for 100 times for most points. For one point in each sub-figure, the simulations were run 1000 times. Thus, points marked as 100% with a star (indicate a better than 99.9% switch for 100 nm and 50 nm lateral dimension as there are no failure for 1000 runs). However, for 20 nm case, 19 failures in 1000 runs at pulse width of 7 ps indicate ~98% switching].

C. Switching Energy Per Bit

Considering an application of a voltage pulse of 2.0 V for a 1.2 nm thick free layer and a 1 nm thick MgO layer with relative permittivity ~ 7, energy dissipated per switching event in a 100 nm nanomagnet is ~1fJ. Sub 1 fJ/bit switching for 20nm

nanomagnet can be achieved (provided large VCMA co-efficient, PMA and DMI are available) which is highly desirable for energy efficient memory devices.

IV. CONCLUSION

In summary, our simulations show that thermally robust switching with a frequency of 2 GHz can be attained for a 100 nm nanomagnet. This switching remains robust when scaling down to 50 nm lateral dimensions in the presence of thermal noise with a switching frequency of ~20 GHz with appropriate choice of feasible material parameters based on experimentally reported values of VCMA coefficient (370 fJ/Vm) [35], PMA (3700 μ J/m²) [36] and DMI (~3mJ/m²) [37, 38, 39].

Similarly, while downscaling to 20 nm, thermally robust switching with a very large frequency in the range of ~100 GHz can be achieved provided material parameters with large VCMA [40], DMI [41, 42] and PMA [36, 40] are chosen. Among these three parameters only PMA [36] has been experimentally reported, while DMI and VCMA values (for the 20 nm nanomagnet simulation) have only been theoretically predicted [40, 41, 42] to date but not experimentally demonstrated. This is an important challenge in scaling from 50 to 20 nm.

Thus, skyrmion mediated ferromagnetic reversal offers an extremely energy efficient (with dissipation < 1 fJ/bit) alternative to spin transfer torque (STT) random access memory devices (with dissipation ~100 fJ/bit). This scheme scales to lateral dimensions of 50 nm, though further scaling to 20 nm is currently impeded by the large values of DMI, PMA and VCMA needed. For aggressive scaling to 20 nm and below, ferrimagnet systems (rather than ferromagnets) could potentially offer a thermally robust skyrmion mediated switching route with experimentally demonstrated material parameters due to small stray fields and low DMI, PMA and VCMA requirement to form skyrmions [43, 44].

APPENDIX

I. Grid Size Dependence of Non-thermal Evolution of Topological Charge

Switching dynamics depends on grid size. To observe the grid size dependence on switching dynamics, the 100nm MTJ is allowed to oscillate for 20 ns once the PMA has been reduced to $1128~\mu\text{J/m}^2$ from $1332~\mu\text{J/m}^2$ within 0.1 ns. As the metastable skyrmion oscillates we compare the dynamics for

 $32\times32\times1$, $64\times64\times1$ and $100\times100\times1$ grid. When the topological charge reaches the peak values PMA is restored to $1332 \,\mu\text{J/m}^2$ and switching is found up to 9, 5 and 4 cycles for $32\times32\times1$, $64\times64\times1$ and $100\times100\times1$ grid respectively (see Fig. 4). However, the dynamics are qualitatively similar for all cases. This shows that the "physics" of skyrmion reversal is affected by the boundary discretization due to different grid sizes and it is not a numerical issue with choice of grid size. In this study we choose $64\times64\times1$ grid for $100 \,\text{nm}$ (each cell of $1.56\,\text{nm}\times1.56\,\text{nm}\times1.2\,\text{nm}$) which best matches typical edge effects due to lithographic imperfections.

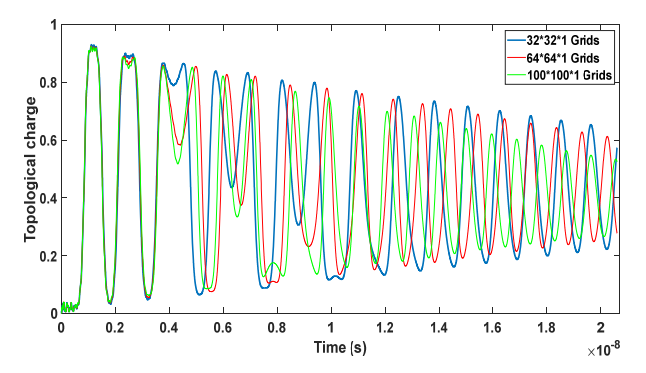


Fig. 4: Evolution of topological charge of 100nm MTJ for $32\times32\times1$, $64\times64\times1$ and $100\times100\times1$ Grids

II. Effect of Time Step Variation on Non-thermal Evolution of Topological Charge

To show the effect of varying time step on switching mechanism, non-thermal evolution of topological charge was observed. For 100 nm MTJ and 64×64×1 grid the evolution of topological charge is shown in Fig. 5 where we can see for all time steps (100fs, 50fs, 10fs, 5fs and adaptive), the time for formation of skyrmion is nearly same but the stability of metastable skyrmion differs. For 100 fs time step, the metastable skyrmion is destroyed as soon as the PMA is restored. For 50 fs the skyrmion breathes for ~ 1ns after the PMA restoration. As the time step size is lowered the evolutionary pattern converges. Thus, we choose time step of 10 fs for all our simulations.

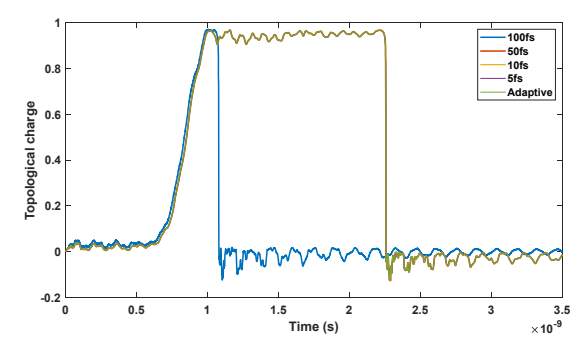


Fig. 5: Evolution of topological charge for different time steps

REFERENCES

- Y. Nakatani, M. Hayashi, S. Kanai, S. Fukami and H. Ohno, "Electric field control of Skyrmions in magnetic nanodisks," Appl. Phys. Lett. 108, Art. No. 152403, Apr. 2016.
- [2] D. Bhattacharya, MM Al-Rashid, J. Atulasimha, "Voltage controlled core reversal of fixed magnetic Skyrmions without a magnetic field," *Scientific Reports* vol. 6, Art. No. 31272, Aug. 2016.
- [3] D. Bhattacharya, S. Razavi, H. Wu, B. Dai, K. Wang, J. Atulasimha, "Creation and annihilation of non-volatile fixed magnetic skyrmions using voltage control of magnetic anisotropy," Nature Electronics, June 2020.
- [4] D. Bhattacharya and J. Atulasimha, "Skyrmion-mediated voltage-controlled switching of ferromagnets for reliable and energy-efficient two-terminal memory," ACS Appl. Mater. Interfaces, Vol. 10(20), pp.17455-17462, May 2018.
- [5] T. Valet and A. Fert, "Theory of the perpendicular magnetoresistance in magnetic multilayers," Phys. Rev. B, Vol. 48(10), pp.7099-7113, Sept. 1993.
- [6] J. S. Moodera, Lr Kinder, TM Wong, R. Meservey, "Large magnetoresistance at room temperature in ferromagnetic film tunnel junctions," Phys. Rev. Lett., Vol. 74(16), pp.3273-3276, Apr. 1995.
- [7] T. Miyazaki and N. Tezuka, "Giant magnetic tunneling effect in Fe/Al₂O₃/Fe junction," Journal of magnetism and magnetic materials, Vol. 139(3), pp.L231-L234, Jan. 1995.
- [8] S S P Parkin, "Giant magnetoresistance in magnetic nanostructures," Annual Review of Materials Science, Vol. 251(1), pp. 357-388, Aug. 1995.
- [9] J. C. Slonczewski, "Current-driven excitation of magnetic multilayers," Journal of Magnetism and Magnetic Materials, Vol. 159(1), pp.L1-L7, Jun. 1996.
- [10] L. Berger, "Emission of spin waves by a magnetic multilayer traversed by a current," Phys. Rev. B, Condensed matter, Vol. 54(13), pp.9353-9358, Oct. 1906
- [11] J. Z Sun, "Current-driven magnetic switching in magnetic trilayer junctions," Journal of Magnetism and Magnetic Materials, Vol. 202(1), pp.157-162, Jun. 1999.
- [12] J. A. Katine, F. J. Albert, R. A. Buhrman, E. B. Myers and D. C. Ralph, "Current-driven magnetization reversal and spin-wave excitations in Co/Cu/Co pillars," Phys. Rev. Lett., Vol. 84(14), pp. 3149-52, Apr. 2000.
- [13] H. Kubota, A. Fukushima, K. Yakushiji, T. Nagahama, S. Yuasa, K. Ando, H. Maehara, Y. Nagamine, K. Tsunekawa, D. Djayaprawira, N. Watanabe, Y. Suzuki, "Quantitative measurement of voltage dependence of spin-transfer torque in MgO-based magnetic tunnel junctions," *Nature Physics*, Vol. 4(1), pp.37–41, Jan. 2008.
- [14] Y. Shiota, T. Nozaki, F. Bonell, S. Murakami, T. Shinjo, Y. Suzuki, "Induction of Coherent Magnetization Switching in a Few Atomic Layers of FeCo Using Voltage Pulses," Nat. Mater., Vol. 11(1), pp.39-43, Jan. 2012.
- [15] P. K. Amiri and K. L. Wang, "Voltage-Controlled Magnetic Anisotropy in Spintronic Devices," Spin, Vol. 02, No. 03, 1240002, Oct. 2012.
- [16] W. Wang, M. Li, S. Hageman, C. L. Chien, "Electric-Field Assisted Switching in Magnetic Tunnel Junctions," Nat. Mater., Vol. 11(1), pp. 64–68, Jan. 2018.
- [17] T. Maruyama, Y. Shiota, T. Nozaki, K. Ohta, N. Toda, M. Mizuguchi, A. A. Tulapurkar, T. Shinjo, M. Shiraishi, S. Mizukami, Y. Ando, Y. Suzuki, "Large Voltage-Induced Magnetic Anisotropy Change in a Few

- Atomic Layers of Iron," Nat. Nanotechnol., Vol. 4(3), pp.158-161, Jan. 2009.
- [18] C. Grezes, F. Ebrahimi, J. G. Alzate, X. Cai, J. A. Catine, J. Langer, B. Ocker, P. K. Amiri, K. L. Wang, "Ultra-Low Switching Energy and Scaling in Electric-Field-Controlled Nanoscale Magnetic Tunnel Junctions with High Resistance-Area Product," Appl. Phys. Lett., Vol. 108(1), Art. No. 012403, Jan 2016.
- [19] W. Kang, Yi Ran, Y. Zhang, W. Lv, W. Zhao, "Modeling and Exploration of the Voltage Controlled Magnetic Anisotropy Effect for the Next-Generation Low-Power and High-Speed MRAM Applications," IEEE Trans. Nanotechnol., Vol. 16(3), pp.387–395, May 2017.
- [20] N. Tiercelin, Y. Dusch, V. Preobrazhensky, P. Pernod, "Magnetoelectric Memory Using Orthogonal Magnetization States and Magnetoelastic Switching," J. Appl. Phys. 109, No. 07D726, Apr. 2011.
- [21] J. Cui, J. L. Hockel, P. K. Nordeen, D. M. Pisani, C. Liang, G. P. Carman and C. S. Lynch, "A method to control magnetism in individual strain-mediated magnetoelectric islands," Appl. Phys. Lett. 103, 232905, Dec. 2013.
- [22] N. D'Souza, M. S. Fashami, S. Bandyopadhyay, J. Atulasimha, "Experimental Clocking of Nanomagnets with Strain for Ultralow Power Boolean Logic," Nano Lett., Vol. 16(2), pp.1069-1075, Feb 2016.
- [23] S. Datta, V. Q. Diep, B. Behin-Aein, "What Constitutes a Nanoswitch? A Perspective," Emerging Nanoelectronic Devices," John Wiley & Sons, 2015, pp 15–34.
- [24] J. G. AlzateVinasco, "Voltage-Controlled Magnetic Dynamics in Nanoscale Magnetic Tunnel Junctions," Ph.D. dissertation, Elect. Eng., Univ. of California, Los Angeles, Los Angeles, CA, USA, 2014. [Online]. Available: https://escholarship.org/uc/item/6wm7x0rf
- [25] Mk Niranjan, CG Duan, SS Jaswal, Ey Tsymbal, "Electric Field Effect on Magnetization at the Fe/MgO(001) Interface," Appl. Phys. Lett., Vol. 96(22), No. 222504, Jun. 2010.
- [26] R. Tomasello, E. Martinez, R. Zivieri, L. Torres, M. Carpentieri and G. Finocchio, "A strategy for the design of skyrmion racetrack memories," *Scientific Reports*, Vol. 4, Art. No. 6784, Oct. 2014.
- [27] X. Zhang, G. P. Zhao, H. Fangohr, J. P. Liu, W. X. Xia, F. J. Morvan, "Skyrmion-skyrmion and skyrmion-edge repulsion in skyrmion-based racetrack memory," *Scientific Reports*, Vol. 5, Art. No. 7643, Jan 2015.
- [28] A. Fert, V. Cros and J. Sampaio, "Skyrmions on the track," *Nature Nanotechnology*, Vol. 8, pp.152–156, Mar. 2013.
- [29] A. Vansteenkiste, J. Leliaert, M. Dvornik, M. Helsen, F. Garcia-Sanchez, B. V. Waeyenberge, "The Design and Verification of MuMax3. AIP Adv. 4, No. 107133, Oct. 2014.
- [30] J. Sampaio, A. V. Khvalkovskiy, M. Kuteifan, M. Cubukcu, D. Apalkov, V. Lomakin, V. Cros, and N. Reyren. "Disruptive effect of Dzyaloshinskii-Moriya interaction on the magnetic memory cell performance," Applied Physics Letters, Vol. 108(11), 112403, Mar. 2016.
- [31] X. Zhao et al., "Enhancing domain wall velocity through interface intermixing in W-CoFeB-MgO films with perpendicular anisotropy," Applied Physics Letters, Vol. 115, 122404, Sep. 2019.
- [32] X. Zhang et al., "Skyrmions in Magnetic Tunnel Junctions," ACS Applied Materials & Interfaces, 10 (19), 16887-16892, Apr. 2018.
- [33] N. E. Penthorn, X. Hao, Z. Wang, Y. Huai, and H. W. Jiang, "Experimental Observation of Single Skyrmion

- Signatures in a Magnetic Tunnel Junction," Phys. Rev. Lett. 122, 257201, June 2019.
- [34] X. Zhang, N. Vernier, W. Zhao, H. Yu, L. Vila, Y. Zhang and D. Ravelosona, "Direct Observation of Domain-Wall Surface Tension by Deflating or Inflating a Magnetic Bubble," Phys. Rev. Applied 9, 024032, Feb. 2018.
- [35] A. Kozio-Rachwa, T. Nozaki, K. Freindl, J. Korecki, S. Yuasa and Y. Suzuki, "Enhancement of perpendicular magnetic anisotropy and its electric field-induced change through interface engineering in Cr/Fe/MgO," Sci. Re., Vol. 7(1), pp.5993, Jul. 2017.
- [36] T. Nozaki, A. Kozio-Rachwa, M. Tsujikawa, Y. Shiota, X. Xu, T. Ohkubo, T. Tsukahara, S. Miwa et al., "Highly efficient voltage control of spin and enhanced interfacial perpendicular magnetic anisotropy in iridium-doped Fe/MgO magnetic tunnel junctions," NPG Asia Materials, Vol. 9(12), pp. e451, Dec. 2017.
- [37] A. Samardak, A. Kolesnikov, M. Stebliy, L. Chebotkevich, A. Sadonikov, S. Nikitov, A. Talapatra, J. Mohanty, A. Ognev, "Enhanced interfacial Dzyaloshinskii-Moriya interaction and isolated skyrmions in the inversion-symmetry-broken Ru/Co/W/Ru films," Appl. Phys. Lett., Vol. 112(19), 192406, May 2018.
- [38] A. Cao, X. Zhang, B. Koopmans, S. Peng, Y. Zhang, Z. Wang, S. Yan, H. Yang and W. Zhao, "Tuning the Dzyaloshinskii-Moriya interaction in Pt/Co/MgO heterostructures through the MgO thickness," Nanoscale, 10, 12062, May 2018.
- [39] A. Cao, R. Chen, X. Wang, X. Zhang, S. Lu, S. Yan, B. Koopmans and W. Zhao, "Enhanced interfacial Dzyaloshinskii-Moriya interactions in annealed Pt/Co/MgO structures," Nanotechnology 31, 155705, Jan. 2020.
- [40] Sohee Kwon, Q. Sun, F. Mahfouzi, Kang L. Wang, P. K. Amiri and N. Kioussis, "Voltage-controlled magnetic anisotropy in heterostructures with atomically thin heavy metals," Physical Review Applied, Vol. 12(4), 044075, Oct. 2019.
- [41] H. Yang, A. Thiaville, S. Rohart, A. Fert and M. Chshiev, "Anatomy of Dzyaloshinskii-Moriya Interaction at Co/Pt interfaces," Physical review letters, Vol. 115(26), pp.267210, Dec. 2015.
- [42] H. Yang, O. Boulle, V. Cros, A. Fert and M. Chshiev, "Controlling Dzyaloshinskii-Moriya interaction via chirality dependent atomic-layer stacking, insulator capping and electric field," Scientific Reports, Vol. 8(1), pp.1-7, Aug. 2018.
- [43] K. Tanaka, S. Miwa, Y. Shiota, N. Mizuochi, T. Shinjo, Y. Suzuki, "Large voltage-induced magnetic anisotropy field change in ferrimagnetic FeGd," Applied Physics Express, Vol. 8(7), pp.073007 (3), June 2015.
- [44] L. Caretta, M. Mann, F. Buttner, K. Ueda, B. Pfau et. al., "Fast current-driven domain walls and small skyrmions in a compensated ferrimagnet," *Nature Nanotech*, Vol. 13(12), pp.1154–1160, Dec. 2018.